Surface-enhanced Raman scattering substrates of high-density and high-homogeneity hot spots by magneto–metal nanoprobe assembling

Lu Zhang,[1] Wen-Fei Dong,[1] Zhi-Yong Tang,[2,5] Jun-Feng Song,[1] Hong Xia,[1] and Hong-Bo Sun[1,3,4]

[1]*State Key Laboratory on Integrated Optoelectronics, College of Electronic Science and Engineering, Jilin University, 2699 Qianjin Street, Changchun 130012, China*

[2]*National Center of Nanoscience and Technology, Beijing 100190, China*

[3]*College of Physics, Jilin University, 119 Jiefang Road, Changchun 130023, China*

[4]*e-mail: hbsun@jlu.edu.cn*

[5]*e-mail: zytang@nanoctr.cn*

Received June 1, 2010; revised September 11, 2010; accepted September 13, 2010; posted September 14, 2010 (Doc. ID 129273); published September 30, 2010

Binary naoparticles composed of a superparamagnetic Fe_3O_4 core and an Au nanoshell were prepared via a high-temperature hydrolysis reaction followed by seed-mediated growth. The nanoprobes render simultaneous dual functions of both fast magnetic response and local surface plasmon resonance. Using these nanoprobes, analyte molecules can be easily biologically captured, magnetically concentrated, and analyzed by surface-enhanced Raman scattering (SERS). Particularly, the complex particles were assembled under magnetic force direction into a SERS substrate. It was found to possess both a high enhancement factor (10^6) and high homogeneity of "hot spot" distribution (fluctuation less than 20% for a 1 μm^2 area) with 4-aminothiophenol as the analyte.

OCIS codes: 160.3820, 170.5660, 240.6695, 280.1545.

Surface-enhanced Raman scattering (SERS) is a highly specific and sensitive optical technique for rapid detection of ultratrace analytes in physiological environments [1–3]. When analyte molecules are absorbed on rough metallic substrates or metal nanoparticle aggregates, collective oscillation of free electrons on the metal surface excited by an incident light, known as localized surface plasmon resonance (LSPR), results in enhanced Raman scattering [1–3]. Particularly, when two metallic nanoparticles are in close proximity, their dipole coupling leads to enhancement factors as high as 10^6–10^{14} [4]. Therefore, numerous active SERS sensors, including metallic or semiconducting nanoparticles and their arrays [5], island films, grating substrates, and metal-coated SiO_2 films, have been utilized in *in vitro* or *in vivo* biomedical measurements [3,6]. For *in vivo* detection of analytes in both living cells and physiological flows, surface modified metal nanoparticles are considered a promising tool. However, introduction of nanoparticles into circulatory systems poses health risks to the living cells or tissues, and their potential toxicity is not fully understood. Thus, the recycling ability of nanoparticles becomes one of the important prerequisites for *in vivo* measurements. To this end, magneto–metal binary nanoprobes, composed of magnetic cores with metal shells, have been developed by many groups [7]. An open problem currently encountered is that individual magneto–metal nanoprobes carrying desired analyte molecules exhibit rather weak SERS, as compared with the smaller-sized metal nanoparticles or nanoparticle aggregates. This is mainly due to the lack of hot spots (the interparticle gaps) on colloid surfaces. To solve this problem, we develop a simple approach to preparing magneto–metal nanoprobes composed of a Fe_3O_4 core and an Au nanoshell. We further assemble the nanoprobes into a SERS substrate of high-density and high-homogeneity "hot spots" by magnetic-directed self-assembly, from which a significantly enhanced SERS signal is attained.

The magneto–metal nanoprobes were synthesized by a simple seed-mediated method [8]. First, the Fe_3O_4 nanoparticles, produced by a high-temperature hydrolysis reaction [9], were coated with uniform shells of amorphous silica. Then Au seeds were attached onto the Fe_3O_4–silica nanoparticles. Prior to the growth of Au nanoshells, certain amounts of $HAuCl_4$ and K_2CO_3 in aqueous solution were added into the Au-seed-coated Fe_3O_4 nanoparticle solution. The formation of magneto–metal nanoprobes was triggered by injecting HCHO into the mixture solution. As shown in Fig. 1(a), core-shell nanoparticles have a uniform diameter of around 170 nm after a 30 min reduction reaction. By increasing the reduction time to 50 min, rougher and thicker Au nanoshells were obtained [Fig. 1(c)]. The elemental signals of Au dramatically increased with the reaction time, and the intensity ratio of Au/Si in Fig. 1(d) is 10 times higher than that in Fig. 1(b). The saturation magnetization of the nanoprobes reached 12 emu/g, and there is no remanence or coercive forces [Fig. 1(e)] displaying superparamagnetic behavior at room temperature. When a magnetic field is applied on one side of the vial, the nanoprobes quickly move to the vial wall within a few seconds [Fig. 1(e)]. After releasing the magnetic force, gentle shaking or ultrasonic vibration led to a rapid redispersion without any aggregation.

The surface plasmon resonances (SPRs) of these magneto–metal nanoprobes, monitored by UV–visible absorption spectra, were to some degree designable by controlling the reduction reaction time. The SPR peak obviously shifts from 580 to 880 nm when the Au-reducing reaction time is increased from 10 to 50 min, just as the near-IR absorption intensity increases [Fig. 2(a)]. The 300 nm redshift of the SPR peak can be attributed to the

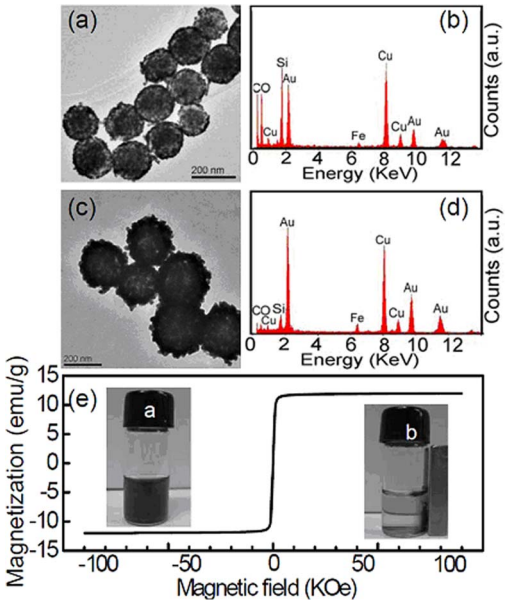

Fig. 1. (Color online) Transmission electron microscopy images of the Fe_3O_4 core with a (a) thin and a (c) thick Au shell. (b) and (d) are the corresponding energy-dispersive spectrum analysis. (e) Hysteresis loops recorded at 300 K of nanoprobes. The inset photographs are of the nanoprobe suspension before (inset a) and after (inset b) magnetic separation.

increase of the thickness of the Au shell [10] and the aggregates of Au nanoparticles on the Au shell surface [11]. The absorption peak of the nanoprobes used was about 770 nm. The probe molecule 4-aminothiophenol (ATP)

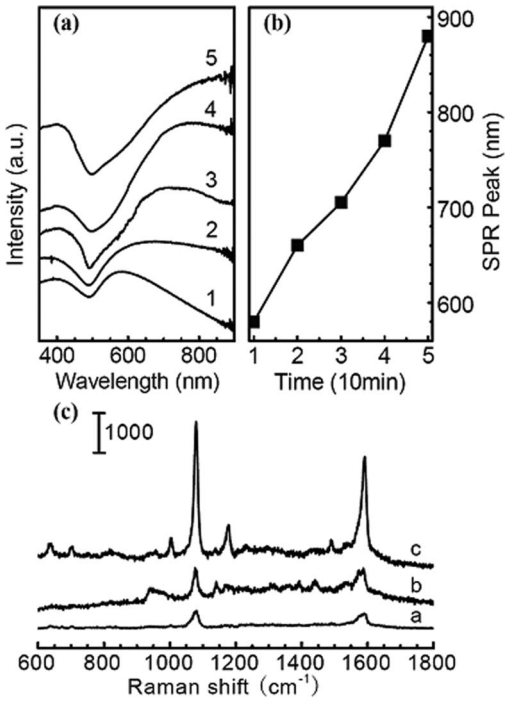

Fig. 2. (a) UV–visible absorption spectra of the Fe_3O_4 core/Au shell nanoprobes after the first to fifth Au-reducing reactions. (b) Shift in the SPR peak position of Au nanoprobes, showing the tunability of SPR of the nanoprobes. (c) SERS spectra of 10^{-6} M ATP on the separate nanoprobes (curve a), and on randomly aggregated nanoprobes at 633 (curve b) and 785 nm (curve c) excitation.

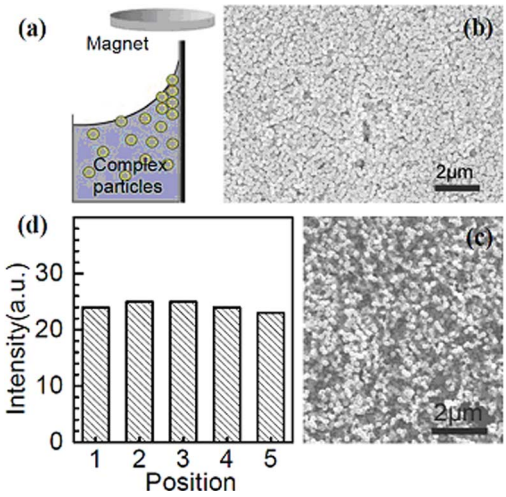

Fig. 3. (Color online) (a) Sketch map of the magnetic-assembly procedure. SEM images of the (b) magnetic-assembled film and (c) randomly aggregated film of Fe_3O_4 core/Au shell nanoprobes. (d) Area chart of the number of the magnetic-assembled nanoprobes per μm^2 in the SEM image of (b).

of 10^{-6} M was added into the nanoprobe solution, and then the ATP molecules were captured by the nanoprobes through formation of stable Au—S bonds. Raman measurements were carried out with two lasers of 633 and 785 nm wavelengths as the excitation sources. The laser power used was 1 mW, and the laser spot was 1 μm in diameter. SERS signals do appear [curve a, Fig. 2(c)], but the intensity is very weak, consistent with Zhang *et al.*'s observation [7], which could be mainly due to the lack of hot spots.

To obtain stronger SERS signals, a dropwise mixture aqueous solution of the nanoprobes and ATP was deposited on the silicon surface. Aggregated nanoparticles formed spontaneously on the silicon surface after water evaporation. The Raman signals were greatly improved for both laser wavelengths, but the enhancement of nanoprobes to ATP at 785 nm [curve c, Fig. 2(c)] is obviously greater than that at 633 nm (curve b). Raman scattering enhancement on Au is difficulty at wavelengths below 620 nm [12]. What's more, the coincidence between the incident radiation and the electronic absorption maxima should contribute to greater SERS enhancement on nanostructures [13], and the resonance is expected to occur at a wavelength longer than that of the LSPR of individual

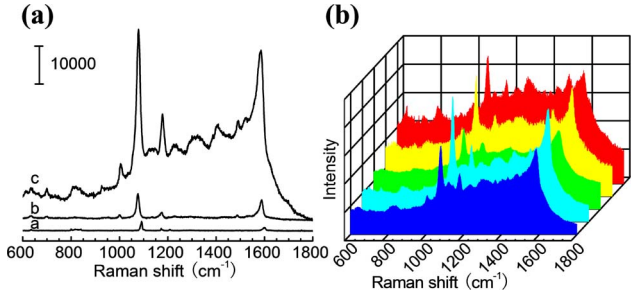

Fig. 4. (Color online) (a) Normal Raman spectrum of ATP in a solid sample (curve a). SERS spectra of 10^{-6} M ATP on randomly aggregated Fe_3O_4 core/Au shell nanoprobes (curve b) and magnetic-assembled nanoprobes (curve c) at 785 nm excitation. (b) SERS spectra of 10^{-6} M ATP on the magnetic-assembled nanoprobes collected at five random spots.

particles [14]. Thus, 785 nm is an appropriate laser wavelength for investigating SERS behaviors. The most intense peak at 1090 cm^{-1} is the bending vibration of C—S, which is assigned to the a_1 mode of ATP aromatic ring vibrations. We use the enhancements to δ_{CS} to estimate the enhancement factor, η according to the definition $\eta = (I_{SERS}/N_{ads})/(I_{bulk}/N_{bulk})$, where I_{SERS} and I_{bulk} are, respectively, the Raman signals of δ_{CS} at 1090 cm^{-1}. N_{ads} and N_{bulk} are the numbers of the absorbed and the solid ATP molecules under the laser illumination volume, respectively. For ATP solids, the diameter of the laser spot area is about 1 μm, and the penetration depth is about 25 μm. N_{bulk} was calculated as about 9.41×10^{10} molecules. N_{ads} was calculated according to the method proposed by Orendorff *et al.* [13], i.e., $N_{abs} = N_d A_{laser} A_N/\sigma$, where N_d (10 nanoparticles/μm^2) is the number density of the composite nanoparticles, A_{laser} is the irradiated area (0.25π μm^2), A_N (3.14×10^{-2} μm^2) is the average top area of a nanoparticle, and σ(0.2 nm^2) is the surface area occupied by an ATP molecule [15]. So we thus obtain that $\eta = 2.5 \times 10^5$. Such a high enhancement factor should be originated from the strong localized electromagnetic field produced by the gaps between two neighboring particles.

Although significant enhancement has been observed, the enhancement factors varied by orders of magnitude when measurement was conducted on different points of concern on the substrate of random nanoparticle aggregate, which is undesirable for quantitative determination of trace analytes. Aided with a magnet, a magnetically directed self-assembling method [Fig. 3(a)] was proposed to densify the nanoprobes in the aggregated film [Fig. 3(b)]. As a result, the average number of nanoparticles per μm^2 (and, therefore, the hot spot density) is twice increased, implying a 4 times larger enhancement factor compared with the spontaneously aggregated samples. Interestingly, we experimentally attained $\eta = 3.0 \times 10^6$ [curve c, Fig. 4(a)], 1 order of magnitude greater than that from spontaneously aggregated film [curve b, Fig. 4(a)]. The approximately 2.5 times extra enhancement compared with the estimation of pure hot spot density calculation should be a result of modified interparticle gaps. It is well known that smaller interparticle distance and sharper curvature of hot sites leads to larger electromagnetic enhancement. More importantly, the density and the homogeneity of hot spots were significantly improved. SERS spectra of ATP on the sample collected at a random five spots on the magnetically directed self-assembled substrate [Fig. 4(b)] exhibit a standard deviation of less than 20% across the entire substrate.

In conclusion, magnetic core gold shell binary nanoprobes were synthesized by a high-temperature hydrolysis reaction followed by a well-controlled seed-mediated approach. It is possible that the nanoprobes could be distributed into human circulatory systems to capture target analytes and then be recycled. The recycled nanoprobes could be assembled under externally exerted magnetic force into a SERS substrate consisting of highly dense and remarkably homogenous hot spots. The proposed method would be greatly advantageous to ultratrace analyte separation, concentration, and high-sensitivity detection for rapid medical diagnosis.

The authors thank the National Natural Science Foundation of China (NSFC) for support under grants 60977056, 60877019, and 90923037.

References

1. T. W. Koo, S. Chan, and S. A. A. Berlin, Opt. Lett. **30**, 1024 (2005).
2. M. E. Stewart, C. R. Anderton, L. B. Thompson, J. Maria, S. K. Gray, J. A. Rogers, and R. G. Nuzzo, Chem. Rev. **108**, 494 (2008).
3. M. M. Dvoynenko and J. K. Wang, Opt. Lett. **32**, 3552 (2007).
4. M. I. Stockman, Top. Appl. Phys. **103**, 47 (2006).
5. H. H. Wang, C. Y. Liu, S. B. Wu, N. W. Liu, C. Y. Peng, T. H. Chan, C. F. Hsu, J. K. Wang, and Y. L. Wang, Adv. Mater. **18**, 491 (2006).
6. D. A. Stuart, J. M. Yuen, N. S. O. Lyandres, C. R. Yonzon, M. R. Glucksberg, J. T. Walsh, and R. P. Van Duyne, Anal. Chem. **78**, 7211 (2006).
7. Q. Zhang, J. P. Ge, J. Goebl, Y. X. Hu, Y. G. Sun, and Y. D. Yin, Adv. Mater. **22**, 1905 (2010).
8. W. X. Niu, S. L. Zheng, D. W. Wang, X. Q. Liu, H. J. Li, S. Han, J. A. Chen, Z. Y. Tang, and G. B. Xu, J. Am. Chem. Soc. **131**, 697 (2009).
9. H. Xia, L. Zhang, Q. D. Chen, L. Guo, H. H. Fang, X. B. Li, J. F. Song, X. R. Huang, and H. B. Sun, J. Phys. Chem. C **113**, 18542 (2009).
10. C. S. Levin, C. Hofmann, T. A. Ali, A. T. Kelly, E. Morosan, P. Nordlander, K. H. Whitmire, and N. J. Halas, ACS Nano **3**, 1379 (2009).
11. S. L. Westcott, S. J. Oldenburg, T. R. Lee, and N. J. Halas, Chem. Phys. Lett. **300**, 651 (1999).
12. G. C. Schatz, Acc. Chem. Res. **17**, 370 (1984).
13. C. J. Orendorff, A. Gole, T. K. Sau, and C. J. Murphy, Anal. Chem. **77**, 3261 (2005).
14. J. W. Zheng, Y. G. Zhou, X. W. Li, Y. Ji, T. H. Lu, and R. A. Gu, Langmuir **19**, 632 (2003).
15. K. Kim and J. K. Yoon, J. Phys. Chem. B **109**, 20731 (2005).